Analysis of the recombination mechanisms in silicon solar cells with the record 26.6% photoconversion efficiency

1st Anatoliy Sachenko[a] sach@isp.kiev.ua
2nd Vitaliy Kostylyov[a] vkost@isp.kiev.ua
3rd Viktor Vlasiuk[a] viktorvlasiuk@gmail.com
4th Igor Sokolovskyi[a] i.o.sokolovskyi@gmail.com
5th Mykhaylo Evstigneev[b] mevstigneev@mun.ca

[a]*V. Lashkaryov Institute of Semiconductor Physics, National Academy of Sciences of Ukraine, Kyiv, Ukraine*
[b]*Department of Physics and Physical Oceanography, Memorial University of Newfoundland, St. John's, NL, A1B 3X7, Canada*

2021 IEEE 48th Photovoltaic Specialists Conference (PVSC) | 978-1-6654-1922-2/21/$31.00 ©2021 IEEE | DOI: 10.1109/PVSC43889.2021.9519055

***Abstract*—The performance of high-efficiency textured silicon solar cells is modelled within the thin-base approximation. In addition to the standard recombination mechanisms (Shockley-Read-Hall, radiative, and Auger), our approach includes the trap-assisted exciton Auger recombination and the space charge region recombination. A simple phenomenological expression is used for the photocurrent external quantum efficiency in the long-wavelength part of the absorption spectrum. The key parameters of textured silicon solar cells, such as short-circuit current, open-circuit voltage and photoconversion efficiency, are determined theoretically. They are in good agreement with the experimental results obtained for the heterojunction solar cells with the record efficiency of 26.6 % produced by Yoshikawa et al. (2017). The theoretical optimal doping level and base thickness of these solar cells are found to be quite close to the experimental ones.**

***Index Terms*—silicon, solar cell, efficiency, recombination, texture**

I. Introduction

Improving the photoconversion efficiency is a key scientific and practical task in solar cells (SCs) research. It is achieved by reducing the bulk and surface recombination rates and optical losses due to light reflection from the front surface. The bulk recombination rate is decreased by decreasing the SC base thickness and by using high-purity silicon with low concentration of deep impurities responsible for Shockley-Reed-Hall (SRH) recombination. The surface recombination velocity is lowered by using an isotype transition or a heterojunction at the rear SC surface, by surface passivation with thermal silicon oxide or by embedding hydrogen into the semiconductor. Finally, a radical method of decreasing the light reflection coefficient is by texturing the front surface of the silicon wafer.

The purpose of this work is to refine the existing models of silicon SCs by accounting for two effects which are usually neglected. The first one is the nonradiative exciton Auger recombination assisted by deep impurities. Its existence has been unequivocally demonstrated by Hangleiter [1], [2], and its contribution to the net recombination rate is comparable to other recombination channels. In the monograph [3], a detailed analysis of the works [1], [2] was performed from the standpoint of the manifestation of this recombination mechanism. The second effect is recombination in the space-charge region (SCR), which likewise significantly affects the characteristics of silicon SCs.

When considering recombination in the space charge region, the curves of the generation-recombination current on the applied voltage are usually analyzed to single out the contributions of different recombination channels to the current depending on the excess concentration of electron-hole pairs. In this work such analysis is carried out for the SC results reported in [4]. Surprisingly, the experimental lifetime vs. excitation has a maximum at the excess concentration exceeding the doping level [4]. Here, two possible reasons for this non-monotonicity are proposed: (i) it can be interpreted as resulting from a Gaussian distribution of the inverse lifetime in the SCR; (ii) another possible origin of the effective lifetime maximum has to do with bulk SRH recombination assisted by gold impurities; this possibility is discussed in the last section of this work. Both assumptions can quantitatively reproduce the experimental photoconversion parameters to a very high accuracy. A possible way to distinguish between the two recombination mechanisms is proposed in the end of this work.

The theory described below is a one-dimensional approximation, which allows obtaining the values of the photoconversion efficiency and other SC parameters, such as short-circuit current, open-circuit voltage, and the fill factor of the I-V curve. It is valid if two criteria are fulfilled: (i) The diffusion length must be much greater than one-quarter of the base thickness, $L_d >> d/4$; (ii) The net (front plus rear) surface recombination velocity must be much smaller than twice the ratio of the ambipolar diffusion coefficient to the base thickness, $S_s << 2D_A/d$. Then, the spatial dependence of the excess carriers concentration can be neglected. Silicon solar cells with photoconversion efficiency above 20% have a lifetime of more than 1 ms and surface recombination velocity

in the cm/s range. Therefore, they meet both criteria very well.

The results of this theoretical modeling are compared with the experimental results obtained in the work [4], [5] that reports the highest photoconversion efficiency for silicon SCs obtained to date, which at the time of publication was 26.6 %. A good agreement with the experimental results is obtained. It is suggested that efficiency decrease with decreasing the excess concentration, Δn, at low Δn may have to do with the recombination in the space-charge region or with SRH recombination on gold impurities.

II. External quantum efficiency and the light-generated current

The external quantum efficiency $EQE(\lambda)$ allows to determine the photocurrent density generated by the incident radiation with the spectral photon flux $I(\lambda)$ as

$$J_L = q \int d\lambda \, EQE(\lambda) \, I(\lambda) \tag{1}$$

where q is the elementary charge. The value of $EQE(\lambda)$ is determined by such factors as the chemical composition and morphology of the semiconductor surface, coating by transparent conductive or translucent layers or a grid for current collection, the light absorption coefficient in the semiconductor, etc.

The external quantum efficiency is given by the product of absorbance, $A(\lambda)$, and the probability for a photon to enter the SC, $EQE = A(1-R)$, where $R(\lambda)$ is the reflection coefficient. In [6], [7], a theoretical approach is introduced, which allows obtaining J_L from the experimental $R(\lambda)$ curve and a fitting expression for $A(\lambda)$ that involves three parameters. We used a simplified approach [8], [9], in which the short-circuit current is represented by a sum of two contributions:

$$\begin{aligned} J_L = & q \Bigg(\int_{\lambda_0}^{800\,\mathrm{nm}} d\lambda I(\lambda) \, EQE_s(\lambda) \\ & + \int_{800\,\mathrm{nm}}^{1200\,\mathrm{nm}} d\lambda I(\lambda) \, EQE_l(\lambda) \Bigg) \ . \end{aligned} \tag{2}$$

The $EQE(\lambda)$ curve in the long-wavelength (subscript l) part of the spectrum, $\lambda > 800\,\mathrm{nm}$, is fitted with a formula that involves two parameters, f and g:

$$EQE_l(\lambda, d) = \frac{f}{1 + (g\alpha(\lambda)d)^{-1}} \ , \tag{3}$$

where d is the base thickness and $\alpha(\lambda)$ the absorption coefficient. In [8], [9], the fit parameter g was expressed in term of another fit parameter, b, as $g = 4n_r^2/b$. Given that the refractive index, $n_r(\lambda)$, depends very weakly on the wavelength in this part of the spectrum, the two fitting expressions are practically the same.

In the short-wavelength part of the spectrum, $\lambda < 800\,\mathrm{nm}$ (subscript s), the $EQE(\lambda)$ curve does not depend on the thickness. Rather, it is determined by the reflection losses, shading and light absorption outside the base region. Hence, $EQE_s(\lambda)$ at any base thickness can be determined from the experimental plot measured for one base thickness value. The values of EQE_l and $EQEs$ must be the same at $\lambda = 800\,\mathrm{nm}$, which allows to determine the parameter f.

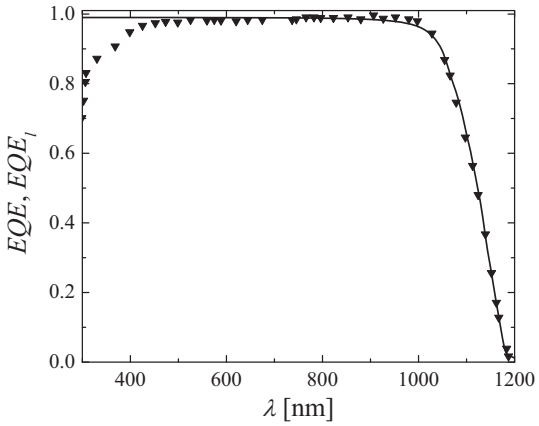

Fig. 1. Experimental external quantum efficiency from [4] (symbols) and theoretical fit with (3) (line).

Figure 1 shows the experimental $EQE(\lambda)$ plot from [4] and a fit $EQE_l(\lambda)$ counterpart. The agreement between the experiment and the fitting expression is achieved for $g = 27.9$ and $f = 0.99$.

III. Recombination mechanisms

The total lifetime τ_{eff} is formed by the intrinsic – radiative and Auger, lifetimes τ_r and τ_A, respectively – and extrinsic recombination processes. The latter includes the SRH recombination with the lifetime τ_{SRH}, the nonradiative excitonic Auger recombination via a deep recombination level [1], [2], [10] with the lifetime τ_{exc-A}, surface recombination and recombination in the space charge region with the lifetimes τ_s and τ_{SCR}:

$$\begin{aligned} \tau_{eff}^{-1} &= \tau_r^{-1} + \tau_A^{-1} + \tau_{extr}^{-1} \ , \\ \tau_{extr}^{-1} &= \tau_{SRH}^{-1} + \tau_{exc-A}^{-1} + \tau_s^{-1} + \tau_{SCR}^{-1} \ . \end{aligned} \tag{4}$$

The radiative recombination lifetime is given by [11]

$$\tau_r^{-1} = B(1 - P_{PR})(n_0 + \Delta n) \ , \tag{5}$$

where B is the radiative recombination coefficient, P_{PR} is the reabsorption probability, n_0 is the equilibrium electron concentration, and Δn the excess electron-hole pair concentration. The radiative recombination coefficient B is expressed by a formula [11]

$$B = \int_0^\infty dE \, B(E) \ , \ \ B(E) = \left(\frac{n_r(E)\alpha(E)E}{\pi c \hbar^{3/2} \, n_i} \right)^2 e^{-E/k_B T} \ , \tag{6}$$

in which $n_r(E)$ and $\alpha(E)$ are the refractive index and absorption coefficient, both depending on photon energy $E = hc/\lambda$. The photon reabsorption probability is given by

$$P_{PR} = B^{-1} \int_0^\infty dE \, A_{bb}(E) \, B(E) \ . \tag{7}$$

The absorbance is given by the same expression as (3), except for the factor f in the numerator is replaced with 1:

$$A_{bb}(E) = \frac{1}{1 + (g\alpha(E)d)^{-1}} \ . \tag{8}$$

For the Auger interband recombination lifetime, we used the empirical expression from [12].

The Shockley-Reed-Hall lifetime as a function of the doping and excitation levels is given by the standard formula

$$\tau_{SRH} \cong \frac{\tau_{p0}(n_0 + n_1 + \Delta n) + \tau_{n0}(p_1 + \Delta n)}{n_0 + \Delta n} \tag{9}$$

Here the characteristics times $\tau_{p0} = (V_p \sigma_p N_t)^{-1}$ and $\tau_{n0} = (V_n \sigma_n N_t)^{-1}$ are expressed in terms of the hole and electron thermal velocities V_p and V_n and their capture cross-sections σ_p and σ_n by the deep traps with concentration N_t. The parameters n_1 and p_1 are the electron and hole equilibrium concentrations in the case when the Fermi energy coincides with the energy level of the trap. Depending on the excess concentration Δn of the electron-hole pairs, the τ_{SRH}-value varies between the low-injection and the high-injection limits. In particular, for SCs with the n-type base, the value of τ_{SRH} increases with Δn for $\sigma_p > \sigma_n$ and is practically constant for $\sigma_p < \sigma_n$.

The nonradiative exciton Auger recombination time is [2]

$$\tau_{exc-A} = \tau_{SRH} \frac{n_x}{n_0 + \Delta n} \tag{10}$$

with [10] $n_x = 8.2 \cdot 10^{15}\,\mathrm{cm}^{-3}$.

The surface and SCR recombination times are defined as

$$\tau_s = \frac{d}{S_s} \ , \quad \tau_{SCR} = \frac{d}{S_{SCR}} \ , \tag{11}$$

where S_s is the net recombination velocity and S_{SCR} is the SCR recombination velocity. For the former, we use the fitting expression:

$$S_s = S_{0s} \frac{n_0}{n_r} \left(1 + \frac{\Delta n}{n_0}\right)^r \ , \tag{12}$$

with the reference concentration $n_r = 6.51 \cdot 10^{14}\,\mathrm{cm}^{-3}$ being the doping level used in [4]. This expression involves two fit parameters: S_{0s} and r, with the latter expected to be of the order of unity.

The SCR recombination velocity is given by a general expression

$$S_{SCR} = \int_0^\infty dx \, \frac{n_0 + \Delta n}{\tau_{SCR}(x)} \Big((n_0 + \Delta n) e^{y(x)} + n_i e^{E_t/kT} + b_r \left((p_0 + \Delta n) e^{-y(x)} + n_i e^{-E_t/kT} \right) \Big)^{-1} \tag{13}$$

Here, the SCR recombination $\tau_{SCR}(x)$ is related to the concentration of traps, $N_t(x)$, as $\tau_{SCR}(x) = 1/(V_p \, \sigma_p \, N_t(x))$, the ratio of the hole-to-electron capture rate constants $b_r = V_p \sigma_p / (V_n \sigma_n)$ is expressed in terms of the electron and hole thermal velocities and capture cross-sections, $V_{n,p}$ and $\sigma_{n,p}$. The trap energy E_t is measured from the middle of the bandgap. Finally, $y(x)$ is the electric potential normalized to the thermal voltage $k_B T/q$. As shown below, a good agreement with the experiment [4] can be achieved by assuming a Gaussian distribution of traps, resulting in a Gaussian distribution of the inverse lifetime with the fit parameters x_m, σ, and τ_m,

$$\tau_{SCR}^{-1}(x) = \tau_m^{-1} \, e^{-(x - x_m)^2/(2\sigma^2)} \ . \tag{14}$$

The upper integration limit w in (13) was taken to be $x_m + 5\sigma$ to make sure that the Gaussian (14) at $x = w$ is practically zero.

To find the dependence of the non-dimensional potential $y(x)$ on the coordinate x, it is necessary to use the solution of the Poisson equation

$$x = \sqrt{\frac{\epsilon_0 \epsilon_{\mathrm{Si}} k_B T}{2 q^2 n_0}} \int_{y_0}^{y} \frac{dy'}{\sqrt{\left(1 + \frac{\Delta n}{n_0}\right)(e^{y'} - 1) - y' + \frac{\Delta n}{n_0}(e^{-y'} - 1)}} \ , \tag{15}$$

where ϵ_0 the vacuum permittivity, and ϵ_{Si} the dielectric constant of Si. The initial value of the potential, $y_0 = y(x = 0)$, is found by modeling the $n - p^+$ junction on the p^+-side as a thin negatively charged slab with the surface charge density $-qN$, N being the surface concentration of acceptor ions in that slab. Then, from the Poissons equation, we find

$$qN = \sqrt{2kT\varepsilon_0 \varepsilon_{\mathrm{Si}}} \sqrt{(n_0 + \Delta n)(e^{y_0} - 1) - n_0 y_0 + \Delta n (e^{-y_0} - 1)} \ . \tag{16}$$

In crystalline n-Si used to manufacture textured SCs, the behavior of $\tau_{eff}(\Delta n)$ in the low-injection region $\Delta n < 10^{14}\,\mathrm{cm}^{-3}$ depends on the passivation of the sample surface. For the samples passivated with SiN_x, the curves $\tau_{eff}(\Delta n)$ saturate, whereas in the samples passivated with Al_2O_3, τ_{eff} increases with Δn and reaches a maximum at $\Delta n \approx 10^{15}\,\mathrm{cm}^{-3}$ (see Fig. 4(b) of [12]). This difference can be attributed to the presence of the surface depletion layer in the latter samples. In SCs, the p-n junction at one of the surfaces necessarily has a SCR, which has the same effect as the depletion layer in the Al_2O_3-passivated n-Si.

It should be noted that the initial increase of $\tau_{eff}(\Delta n)$ with $\Delta n < 10^{14}\,\mathrm{cm}^{-3}$ can also be obtained without invoking the SCR recombination, provided that τ_{SRH} increases with increasing Δn, which is possible if $\sigma_p \geq \sigma_n$. At the end of the work, this case will be analyzed.

IV. Photoconversion efficiency modeling for AM1.5 irradiation

We consider a SC based on a p^+-n-n^+ structure. If the minority carriers diffusion length $L_d = \sqrt{D_A \tau_{eff}}$ is much bigger than one-quarter of the base thickness, $d/4$, and if the combined surface and SCR recombination velocity $S_s + S_{SCR} \ll 2D_A/d$, then the excess concentration profile is practically uniform in the base region. In that case, one

can employ the narrow-base approximation and express the illuminated I-V relation as [9]

$$I(V) = I_L - \frac{qA_{SC}d\Delta n}{\tau_{eff}} - \frac{V + IR_s}{R_{sh}} \ , \qquad (17)$$

where the first term is the photogenerated current, the second term is the recombination current, A_{SC} is the SC area, and R_s and R_{sh} are the series and shunt resistance. The expression for the dark current $I_D(V) = -I(V)|_{I_L=0}$ has the form

$$I_D(V) = \frac{qA_{SC}d\Delta n}{\tau_{eff}} + \frac{V - I_D R_s}{R_{sh}} \ . \qquad (18)$$

The excess carrier concentration is related to the applied voltage by a modified mass action law,

$$(n_0 + \Delta n)(p_0 + \Delta n) = n_{i0}^2 e^{(\Delta E_g + q(V - IR_s))/k_B T} \ . \qquad (19)$$

Here, n_{i0} is the intrinsic concentration at low injection [13], and $\Delta E_g(n_0, \Delta n)$ is the magnitude of bandgap narrowing in Si [14]. The last equation can be solved for the excess concentration:

$$\Delta n = -\frac{n_0}{2} + \sqrt{\frac{n_0^2}{4} + n_{i0}^2 e^{\Delta E_g/k_B T}\left(e^{q(V-IR_s)/k_B T} - 1\right)} \ . \qquad (20)$$

Equations (17), (20) need to be solved numerically.

The relation between the excess concentration Δn_{OC} in the open-circuit mode and the open-circuit voltage V_{OC} is obtained by putting $\Delta n = \Delta n_{OC}$, $V = V_{OC}$, and $I = 0$:

$$\Delta n_{OC} = -\frac{n_0}{2} + \sqrt{\frac{n_0^2}{4} + n_{i0}^2 e^{\Delta E_g/k_B T}\left(e^{qV_{OC}/k_B T} - 1\right)} \ . \qquad (21)$$

The second relation can be obtained from (17) by setting $I = 0$:

$$I_L = \frac{A_{SC}qd}{\tau_{eff}(\Delta n_{OC})}\Delta n_{OC} + \frac{V_{OC}}{R_{sh}} \ . \qquad (22)$$

The photoconversion efficiency η, as well as the voltage, V_m, current, I_m, and output power, $P_m = V_m I_m$, in the maximum-power operation regime are found by setting the derivative of $P = IV$ with respect to voltage to zero.

If we compare the expressions for Δn and Δn_{OC}, as well as the expressions for dark current (18) and photogeneration current (22), we can see that they coincide if we replace $V \to V_{OC}$, $I_D \to I_L$, and set R_s in (20) equal to zero. This means that the expressions for $I_D(V, R_{sh}, R_s = 0)$ and $I_L(V_{OC}, R_{sh}, R_s = 0)$ are identical.

V. Comparison of the Theoretical Modeling with the Experimental Results

Next, we apply the theory above to obtain the main parameters of the textured SCs based on monocrystalline silicon [4]. The key experimental curves presented in [4] were the external quantum efficiency vs. the wavelength $EQE(\lambda)$, the effective lifetime curve vs. the excess concentration of electron-hole pairs $\tau_{eff}(\Delta n)$, the illuminated $I - V$ curves, and the curves of the open-circuit voltage vs. the incident intensity with the AM1.5 spectrum. According to the results presented earlier, the $EQE(\lambda)$ curves obtained in this work with the help of the empirical formula (3) were used to calculate the photogenerated current density J_L. For theoretical modeling of the experimental curves it was necessary to determine a number of unknown parameters, which are not given in [4]. These are the Shockley-Reed-Hall lifetime, the surface recombination rate, the Gaussian parameters that determine the SCR lifetime, the ratio of the capture cross sections for holes and electrons, the shunt resistance and the series resistance.

For simplicity, we initially treat the Shockley-Read-Hall lifetime as a constant fit parameter; in the end, we consider a more accurate model, in which this recombination channel is due to the gold impurities, with τ_{SRH} depending on the excess concentration.

To determine the effective lifetime vs. the excitation level, Yoshikawa et al [4] measured the open-circuit voltage and the short-circuit current for different illumination intensities. When analysing their experimental data, they did not take into account the bandgap narrowing effect. As a result, the open-circuit excess concentration determined in [4], denoted here as Δn_Y, turned out to be slightly underestimated at $\Delta n > 10^{15}\,\mathrm{cm}^{-3}$. To relate the excess concentration Δn_Y from [4] and a more accurate estimate that would take bandgap narrowing into account, we note that the former is given by (cf. Eq. (1) in [5])

$$\Delta n_Y = -\frac{n_0}{2} + \sqrt{\frac{n_0^2}{4} + n_{i0}^2(e^{qV_{OC}/k_B T} - 1)} \ . \qquad (23)$$

The bandgap narrowing $\Delta E_g(\Delta n)$ increases with Δn, but in the relevant parameter range, $\Delta n < 2 \cdot 10^{16}\,\mathrm{cm}^{-3}$ it does not exceed 0.004 eV $\simeq 0.15 k_B T$. This allows to linearize the difference between the expressions (21) and (23) with respect to a small parameter $\Delta E_g/k_B T$ to obtain a more accurate expression for the excess concentration in the open-circuit regime:

$$\begin{aligned} &\Delta n_{OC} - \Delta n_Y \\ &= \frac{\Delta E_g(\Delta n_{OC})}{kT} \frac{\Delta n_Y(N_d + \Delta n_Y) - n_{i0}^2}{\sqrt{n_0^2 + 4(\Delta n_Y(n_0 + \Delta n_Y) - n_{i0}^2)}} \\ &= \frac{\Delta E_g(\Delta n_Y)}{k_B T} \frac{\Delta n_Y(n_0 + \Delta n_Y)}{\sqrt{n_0^2 + 4\Delta n_Y(n_0 + \Delta n_Y)}} \ . \end{aligned} \qquad (24)$$

In the last line, we neglected the intrinsic concentration squared and replaced Δn_{OC} with Δn_Y in the argument of ΔE_g, keeping in mind that the difference between the two estimates for Δn should be quite small.

From the experimental effective lifetime as a function of Δn (see Fig. 4a in [4]), one can determine the "experimental" recombination velocity in the SCR, $S_{SCR}^{exp}(\Delta n)$. For this, one needs the parameters τ_{SRH}, S_{0S}, and r, which can be determined from a comparison between the theoretical and experimental $I - V$ and $\tau_{eff}(\Delta n)$ curves from [4]. Then, one can use an expression

$$\begin{aligned} S_{SCR}^{exp}(\Delta n) = \Big[&\tau_{eff}^{-1} \\ &- \left(\tau_{SRH}^{-1} + \tau_{exc-A}^{-1} + \tau_s^{-1} + \tau_r^{-1} + \tau_A^{-1}\right)\Big] d \ . \end{aligned} \qquad (25)$$

TABLE I
PARAMETERS OBTAINED BY FITTING THE EXPERIMENTAL RESULTS FROM [4]

S_{0s}	r	τ_{SRH}	τ_{SCR}	x_m	σ	b_r	R_s	R_{sh}
0.031 cm/s	2	15.2 ms	14 μs	0.25 μm	45 nm	0.1	0.19 Ω·cm^2	1.48·10^5 Ω·cm^2

Upon substitution of the $\tau_{eff}(\Delta n)$ curve into (25), we obtain the SCR recombination velocity as a function of the excitation level, see Fig. 2 (symbols). The corresponding curve calculated using (13), (14) is shown in Fig. 2 as a solid line. The fit parameters are summarized in Table I. The agreement between the experimental and the fit curves in the range $10^{14}\,\mathrm{cm}^{-3} < \Delta n < 10^{16}\,\mathrm{cm}^{-3}$ is obvious. In turn, the parameters of the Gaussian (14) were found by fitting the $\tau_{eff}(\Delta n)$ curve in the Δn-range to the left of the maximum.

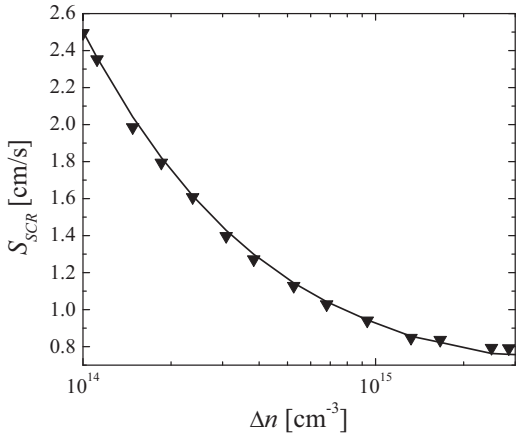

Fig. 2. Experimental (symbols) and calculated (line) SCR recombination velocity vs. excitation level. The experimental data points were infered from [4] using the procedure described in the text.

Let us calculate the $\tau_{eff}(\Delta n_{OC})$ curve more accurately, taking into account the effect of bandgap narrowing, and also find the value of the shunt resistance R_{sh}. To do this, we use the experimental illuminance-open circuit voltage relation from Fig. 4(b) of [4], see Fig. 3. The illumination level is normalized to the value of the sun's illumination for AM1.5 spectrum. The theoretical curve was constructed using the joint solution of equations (21), (22), and the value of the light intensity was obtained by normalizing the photogenerated current density to 0.0425 A/cm^2. The theoretical curve coincided with the experimental one using the fit parameters shown in Table I, in particular, at $R_{sh} = 1.48 \cdot 10^5\,\Omega$·cm^2.

Figure 4 shows the experimental $\tau_{eff}(\Delta n)$ curve (see the blue curve in Fig. 4(a) of [4]). To obtain the theoretical counterpart, we used the expression

$$\tau_{eff} = \frac{qd\,\Delta n_{OC}(V_{OC})}{J_L(V_{OC}) + V_{OC}/R_{sh}} \tag{26}$$

with the dependence $n_{OC}(V_{OC})$ calculated from the joint solution of (21), (22). As can be seen from Fig. 4, at $\Delta n_{OC} <$

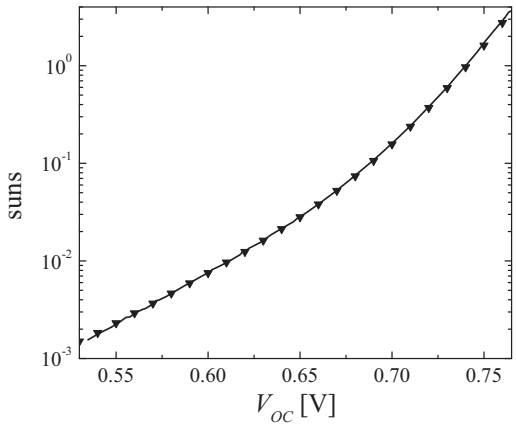

Fig. 3. Illumination versus open-circuit voltage. Symbols: experiment [4], solid line: theoretical fit.

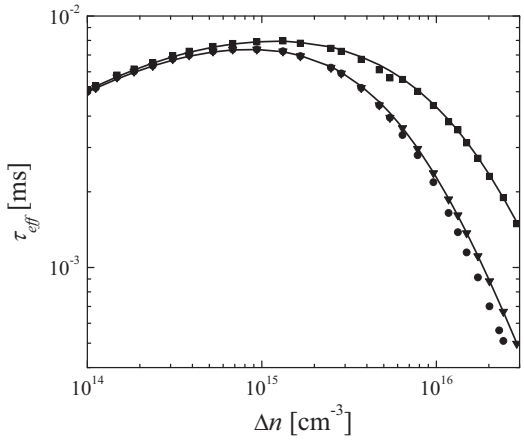

Fig. 4. The effective lifetime as extracted from the experimental data [4] (circles), the corrected effective lifetime (triangles), and the extrinsic recombination time (squares) vs. excess concentration. Solid lines show the theoretical fits.

$10^{15}\,\mathrm{cm}^{-3}$, the calculated curve is consistent with the experimental one from [4]. At the same time, at $\Delta n > 10^{15}\,\mathrm{cm}^{-3}$, the theoretical curve is slightly higher than the dependence from [4]. The reason is that the bandgap narrowing was not taken into account in [4].

The effective lifetime as a function of the excitation level, obtained from Fig. 4(b) of [4] taking into account all possible recombination mechanisms (triangles), and the extrinsic lifetime $\tau_{extr}(\Delta n)$ (rectangles), are shown in Fig. 4. Note that, when calculating the radiative lifetime to obtain

$\tau_{extr} = (\tau_{eff}^{-1} - \tau_r^{-1} - \tau_A^{-1})^{-1}$, we took into account photon reabsorption, whereas in [4], photon reabsorption has been neglected. As can be seen from this figure, as well as from Fig. 4(a) of [4], at excitation levels Δn greater than $10^{16}\,\mathrm{cm}^{-3}$, both curves decrease with almost the same slope. It is easy to see that $\tau_{eff}(\Delta n)$ and $\tau_{extr}(\Delta n)$ are both proportional to Δn^{β}, where β is close to 2. In the case of $\tau_{eff}(\Delta n)$ such a decrease is due to the interband Auger recombination. As for $\tau_{extr}(\Delta n)$ it can only be explained by surface recombination. Therefore, the exponent r in (12) is set to 2.

To understand this exponent, it should be borne in mind that the model of one recombination center close to the middle of the band gap, which is responsible for surface recombination, is approximate. In particular, as studies performed for the Si-SiO_2 system have shown, in addition to discrete levels, there are two systems of continuously distributed donor-like and acceptor-like surface centers [15], [16]. Their concentration, $N_s(E)$ increases exponentially near the edges of the bandgap, and in some instances the contribution of these surface centers to the net recombination rate may exceed the contribution of the deep level [15], [16]. If $\Delta n > n_0$, the electron quasi-Fermi level begins to shift in the direction of increase of $N_s(E)$, and this can lead to an additional increase in $S_s(\Delta n)$ compared to the typical case when $r = 1$. A similar scenario can be realized when crystalline silicon borders on other dielectrics.

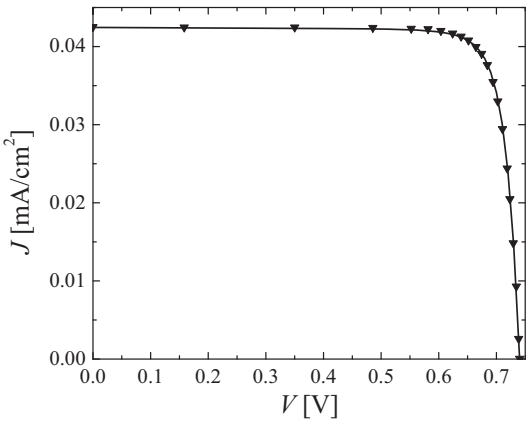

Fig. 5. The experimental [4] current-voltage curve (symbols) and the theoretical fit.

In Fig. 5 the experimental illuminated $J-V$ curves is shown together with the theoretical fitting curve. As can be seen from the figure, the agreement between theory and experiment is good for the parameters given in Table I, in particular, with the series resistance of $0.19\,\Omega{\cdot}\mathrm{cm}^2$.

Using the parameters from Table I and solving jointly (21), (22), we obtained for V_{OC} the calculated value of 740.3 mV, which coincides with the value given in [4]. Substitution of these parameters into the expressions for η and FF, we obtained the calculated values of 26.63 % and 84.65 %, respectively, which also completely agree with the experimental data.

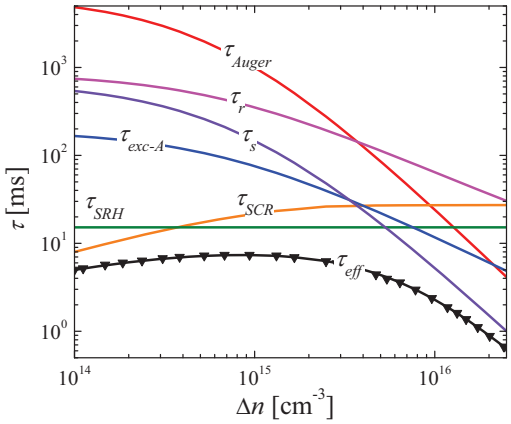

Fig. 6. The effective lifetime together with the individual contributions, as indicated near each curve, vs. the excess concentration. The fit parameters used to generate the theoretical curves are as follows: $\tau_{SRH} = 15.2\,\mu$s, $S_{0s} = 0.031$ cm/s, $r = 2$, $\tau_{SCR} = 14\,\mu$s, $\sigma = 45$ nm, $b_r = 0.1$, $R_{sh} = 1.48 \cdot 10^5\,\Omega{\cdot}\mathrm{cm}^2$, $R_S = 0.19\,\Omega{\cdot}\mathrm{cm}^2$.

As always, the question arises as to how unambiguous the fitting parameters are. At a first glance, the fact that the SRH recombination, surface recombination, and the SCR recombination rates are additive should lead to ambiguity. But each contribution dependens on the excess concentration Δn differently, which eliminates the ambiguity. This point is illustrated in Fig. 6, which, in addition to the dependence $\tau_{eff}(\Delta n)$, shows the individual contributions of all recombination channels considered. As can be seen from Fig. 6, at small values of Δn the greatest contribution to τ_{eff} comes from the SCR and SRH channels, and at large Δn from the Auger and surface recombination. Interestingly, the contributions of exciton non-radiative recombination and radiative recombination depend on Δn in a similar manner, but the contribution of the former is dominating.

Fig. 7 shows the calculated photoconversion efficiency vs. the base doping level at the base thickness $d = 200\,\mu$m. As can be seen from the figure, the maximal efficiency of 26.64% is achieved at $n_0 = 1.5 \cdot 10^{15}\,\mathrm{cm}^{-3}$. It is practically the same as the value used in [4].

Using the model described above, we not only could reach a good agreement with the experimental short-circuit current density of $42.5\,\mathrm{mA/cm}^2$, but also we can calculate the dependence of J_L on the base thickness, which allows to optimize the cell performance with respect to this parameter. Fig. 8 shows the predicted curve $\eta(d)$ based on the so obtained $J_{SC}(d)$ relation. The figure shows that the maximum efficiency of photoconversion is achieved at a base thickness of 80 μm and reaches 26.86 %, exceeding the value from [4] by 0.26 %.

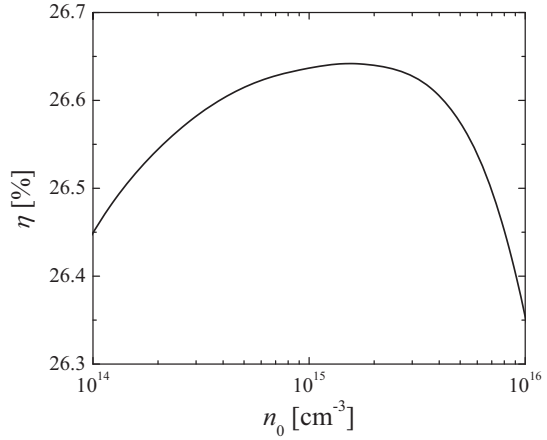

Fig. 7. The theoretical photoconversion efficiency vs. base doping level at the base thickness $d = 200\,\mu$m.

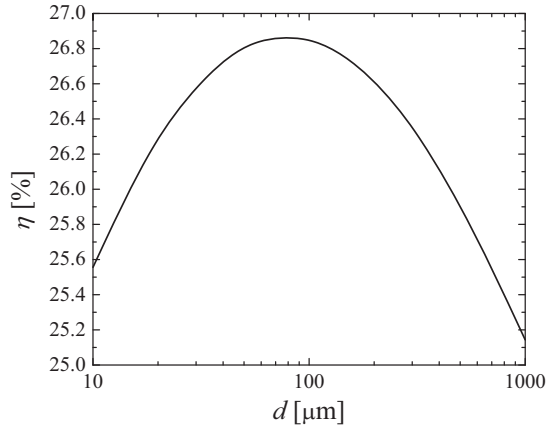

Fig. 8. The theoretical photoconversion efficiency vs. base thickness at the base doping level $n_0 = 6.5 \cdot 10^{14}$ cm^{-3}.

VI. An alternative interpretation of the effective lifetime maximum vs. excess concentration

The maximum of the effective lifetime vs. the excess carrier concentration, Fig. 4, can be explained based on a different set of assumptions. Namely, it can be reproduced by neglecting the SCR recombination completely, and, instead, taking into account the dependence of the bulk SRH lifetime on the excess concentration, assuming that the main impurity responsible for SRH recombination is gold.

The SRH lifetime as a function of the doping and excitation levels is given by

$$\tau_{SRH} = \left(\sum_{i=1}^{2} \frac{N_t(n_0 + \Delta n)}{\frac{n_0 + n_{t,i} + \Delta n}{V_p \sigma_{p,i}} + \frac{p_{t,i} + \Delta n}{V_n \sigma_{n,i}}} \right)^{-1}. \qquad (27)$$

The index i labels the two energy levels of Au trap. The corresponding parameters for Au are given in Graff's monograph [17]: $\sigma_{n,1} = 1.4 \cdot 10^{-16}$, $\sigma_{p,1} = 7.6 \cdot 10^{-15}$, $\sigma_{n,2} = 2.7 \cdot 10^{-15}$, $\sigma_{p,2} = 2.5 \cdot 10^{-15}$ cm^2, $E_{t,1} = -0.55$ eV (measured from the bottom of the conduction band), $E_{t,2} = 0.35$ eV (measured from the top of the valence band), giving $n_{t1} = 1.54 \cdot 10^{10}$ cm^{-3}, $p_{t1} = 6.07 \cdot 10^9$ cm^{-3}; $n_{t2} = 2.64 \cdot 10^6$ cm^{-3}, $p_{t2} = 3.53 \cdot 10^{13}$ cm^{-3}. Finally, the values of average thermal velocities for electrons and holes in silicon are given in [18]: $V_n = 2.04 \cdot 10^7$ cm/s, $V_p = 1.67 \cdot 10^7$ cm/s.

If we set the value of N_t to $3.14 \cdot 10^9$ cm^{-3}, and S_{0s} to 0.0024 cm/s, then the calculated curve of $\tau_{eff}(\Delta n)$ agrees well with the experimental one in the whole range of excess concentrations. In this case, we obtain a theoretical value of V_{OC} equal to 740.3 mV, and setting R_s to 0.135 Ω·cm^2, we obtain the efficiency of 26.63 %. It can be noted that the concentration of gold in silicon of the order of $10^9 - 10^{10}$ cm^{-3} is quite realistic [17].

Thus, for the SCs data from [4], it is not possible to discriminate the mechanisms that provides an initial increase of $\tau_{eff}(\Delta n)$ with Δn. Calculations have shown that this can be explained both by the SCR recombination and recombination in the bulk, for example, with the participation of gold.

Discrimination between the two mechanisms should be possible experimentally from the $\tau_{eff}(\Delta n)$ curve obtained for the material used to create the SC with the appropriately passivated surfaces. In this case, the inversion band bending on them will be absent. If the non-monotonicity of $\tau_{eff}(\Delta n)$ at small Δn still persists, this will signal the bulk Shockley-Read-Hall recombination with the participation of the gold level. If the non-monotonicity is absent, then its presence in the SCs should be attributed to the recombination in the SCR.

VII. Conclusions

The main parameters of high efficiency textured silicon solar cells are modeled within the thin-base approximation. Unlike conventional optimization formalisms, which account for the standard recombination channels, the approach presented here additionally includes such important factors as the non-radiative exciton Auger recombination via deep traps as well as electron-hole pair recombination in the space charge region.

The thin-base formalism allows us describing the experimental results for the heterojunction silicon solar cells with the record photoconversion efficiency of 26.6% from [4]. The expression for the SCR recombination velocity obtained here is valid both at small values of $\Delta n < n_0$ and at $\Delta n > n_0$. It is shown that the contribution of the nonradiative exciton Auger recombination via deep impurities exceeds the contribution of radiative recombination in the SCs analyzed. It is established that the experimentally observed decrease of the effective lifetime $\tau_{eff}(\Delta n)$ at small excess concentrations may be either due to the recombination in the space charge region or due to the SHR recombination via gold impurities. These two recombination mechanisms can be distinguished by measuring $\tau_{eff}(\Delta n)$ on the SC material with well-passivated surfaces, where the SCR is absent.

The simulation results are quantitatively consistent with the experiment across the whole range of parameters. The

results obtained in this work can be used to optimize the characteristics of textured silicon SCs with respect to base doping level and thickness.

ACKNOWLEDGMENT

This work was partially supported (V. Kostylyov, V. Vlasiuk) by the National Research Foundation of Ukraine (project 2020.02/0036: "Development of physical basis of both acoustically controlled modification and machine learning-oriented characterization for silicon solar cells"). M. Evstigneev is grateful to the Natural Sciences and Engineering Research Council of Canada (NSERC) for financial support and to the Atlantic Computational Excellence Network (ACENet) for computational resources.

REFERENCES

[1] A. Hangleiter, "Nonradiative recombination via deep impurity levels in silicon: Experiment", *Phys. Rev. B*, vol. 35 (17), pp. 9149–9160, 1987.
[2] A. Hangleiter, "Nonradiative recombination via deep impurity levels in semiconductors: The excitonic Auger mechanism", *Phys. Rev.B.*, vol. 37(5), pp. 2594-2604, 1988.
[3] V.N. Abakumov, V.l. Perel, I.N. Yassievich, eds., "Nonradlative Recombination in Semiconductors", Elsevier, 1991.
[4] K. Yoshikawa, W. Yoshida, T. Irie, H. Kawasaki, K.I. Konishi, H. Ishibashi, T. Asatani, D. Adachi, M. Kanematsu, H. Uzu , and K. Yamamoto, "Exceeding Conversion Efficiency of 26 % by Heterojunction Interdigitated Back Contact Solar Cell with Thin Film Si Technology", *Solar Energy Materials and Solar Cells*, vol. 173, pp. 37-42, 2017.
[5] K. Yoshikawa, H. Kawasaki, W. Yoshida, T. Irie, K. Konishi, K. Nakano, T. Uto, D. Adachi, M. Kanematsu, H. Uzu and K. Yamamoto, "Silicon Heterojunction Solar Cell with Interdigitated Back Contacts for a Photoconversion Efficiency over 26 %", *Nature Energy*, vol 2, 17032, 2017.
[6] K.R. McIntosh and S.C. Baker-Finch, "A Parameterization of Light Trapping in Wafer-Based Solar Cells", *IEEE J. Photovoltaics*, vol. 5, pp. 15631570, 2015.
[7] A. Fell, K.R. McIntosh, and K.C. Fong, "Simplified Device Simulation of Silicon Solar Cells Using a Lumped Parameter Optical Model", *IEEE J. Photovoltaics*, vol. 6, pp. 611-616, 2016.
[8] A.V. Sachenko, V.P. Kostylyov, A.V. Bobyl, V.M. Vlasyuk, I.O. Sokolovskyi, G.A. Konoplev, E.I. Terukov, M.Z. Shvarts, and M. Evstigneev, "The Effect of Base Thickness on Photoconversion Efficiency in Textured Silicon-Based Solar Cells", *Tech. Phys. Let.*, vol. 44, pp. 873-876, 2018.
[9] A.V. Sachenko, V. P. Kostylyov, V.M. Vlasyuk, I.O. Sokolovskyi, and M. Evstigneev, "Optimization of Textured Silicon Solar Cells", *Proceedings of the 47th IEEE Photovoltaic Specialists Conference* (15-21 June 2020, Calgary, Canada).
[10] A.V. Sachenko, V.P. Kostylyov, V.M. Vlasyuk, I.O. Sokolovskyi , and M. Evstigneev, "The influence of the exciton nonradiative recombination in silicon on the photoconversion efficiency", Proceedings of the 32 European Photovoltaic Solar Energy Conf. and Exhib., Germany, (20 - 24 June 2016. Munich, Germany) Munich. 2016. pp. 141-147.
[11] A. Richter, M. Hermle, and S.W. Glunz, "Reassessment of the Limiting Efficiency for Crystalline Silicon Solar Cells", *IEEE J. Photovolt.*, vol. 3, pp. 1185-1191, 2013.
[12] A. Richter, S. Glunz, F. Werner, J. Schmidt, and A. Cuevas, "Improved quantitative description of Auger recombination in crystalline silicon", *Phys. Rev. B*, vol. 86, pp. 165202:1-14 , 2012.
[13] T. Trupke, M.A .Green, P. Wurfel, P.P. Altermatt, A. Wang, J. Zhao, and R. Corkish, "Temperature dependence of the radiative recombination coefficient of intrinsic crystalline silicon", *J. Appl. Phys.*, vol. 94, pp. 4930-4937, 2003.
[14] A. Schenk, "Finite-temperature full random-phase approximation mode of band gap narrowing for silicon device simulation", *J. Appl. Phys.*, vol. 84, pp. 3684-3695, 1998.
[15] V.P Kostylyov, A.V. Sachenko, I.O. Sokolovskyi, V.V. Chernenko, T.V. Slusar and A.V. Sushyi, "Influence of Surface Centers on the Effective Surface Recombination Rate and the Parameters of Silicon Solar Cells", *Ukr. J. Phys.*, vol 58, pp. 362-369, 2013.
[16] K.R. McIntosh and L.E. Black, "On Effective Surface Recombination Parameters", *J. Appl. Phys.* vol. 116, p. 014503, 2014.
[17] K. Graff, "Metal Impurities in Silicon - Device Fabrication", 2nd ed., Springer, 2000.
[18] M.A. Green, "Intrinsic concentration, effective densities of states, and effective mass in silicon", *J. Appl. Phys.*, vol. 67, pp. 2944 - 2955, 1990.